Performance and Evaluation of Volterra Nonlinear Equalizer for Coherent RoF Mobile Front-haul Network : A case Study of QOSTBCOFDM and QOSTBC-GFDM Waveforms

K. AISSAOUI[1,2], S.Mhatli [1*], O.Gharbi [1,2], Adel Aldalbahi[3], R. Attia[1], S.Haxha[4], I.Dayoub[5]

[1]SERCOM Laboratory, Tunisia Polytechnic School, Carthage University, Tunis 2078, Tunisia
[2]National Engineering School of Tunis, University of Tunis EL MANAR, Tunis 1002, Tunisia
[3]King Faisal University, Hofuf 31982, Saudi Arabia
[4]Microwave Photonics and Sensors, Department of Electronic Engineering, School of Engineering, Physical and Mathematical Sciences, Royal Holloway, University of London, Egham, Surrey, TW20 0EX, UK
[5]Univ. Polytechnique Hauts-de-France, CNRS, Univ. Lille, ISEN, Centrale Lille, UMR 8520 -IEMN - Institut d'Électronique de Microélectronique et de Nanotechnologie,DOAE - Département d'Opto-Acousto-Électronique, F-59313 Valenciennes, France
*Corresponding author: S. Mhatli (sofien_mhatli@yahoo.fr).

Abstract: In this paper, we propose and investigate a multi-Gigabits baseband RF (Radio Frequency) signal over Standard Single-Mode Fibre (SSMF) link using a 16-Quadrature Amplitude Modulation (16-QAM). The proposed novel RF configuration architecture deploys 4x4 Quasi-Orthogonal Space-Time Block Code Generalized Frequency Division Multiplexing (QOSTBC-GFDM) and Orthogonal Frequency Division Multiplexing (QOSTBC-OFDM) waveforms. This configuration can be deployed within the context of fifth-generation (5G) Cloud Radio Access Network (C-RAN). Th eproposed architecture is based on the implementation of a Volterra Nonlinear Equalizer (VNLE) in a Remote Radio Unit (RRU). The equalizer has been efficiently employed to reduce the impact of the non-linear distortion and enhance signal performance. We have used a low-complex Linear Equalizer (LE) at the User Equipment (UE). Our research shows that QOSTBC-GFDM waveform is more efficient than QOSTBC-OFDM in terms of Out-Of-Band (OOB) emission and Spectral Efficiency (SE). Furthermore, a comparable performance between the two waveforms in terms of Bit Error Rate (BER) and Error Vector Magnitude (EVM) is attained. To the best of our knowledge, this is the first reported research work based on precoded QOSTBC-GFDM and QOSTBC-OFDM signal on a fully C-RAN architecture with the integration of the VNLE in the RRU.

Index Terms: C-RAN, MFH, MIMO, QOSTBC-GFDM, QOSTBC-OFDM, RLS, RoF, SSMF, VNLE, 5G & Beyond.

1. Introduction

The International Telecommunications Union Radio communications sector (Recommendation ITU-R M.2083-0) has defined the following three categories of the fifth-generation (5G) of communications networks applications: Enhanced Mobile Broadband (eMBB) to increase mobile broadband capacity at high mobility, massive Machine Type Communication (mMTC) to resolve the massive connectivity issue, and Ultra-Reliable and Low Latency Communication (URLLC), to deliver extremely high reliability with extremely low latency (with 0.5 ms user plane latency). The 5G is launched in the early 2020s and will be envisioned several trillions of devices [1]. The huge number of entities requires high throughput to serve the massive traffic in the network. The new wireless communication standard will support different technologies such as Internet of Things (IoT), Machine to Machine (M2M), Device to Device (D2D), mobile communications, hologram video calls, Augmented Reality (AR), Virtual Reality (VR), tactical internet and high-speed video downloads [2]. Moreover, 5G deployment requires high-density small cell antenna sites, coupled with a C-RAN architecture to handle large traffic volumes, nevertheless still with low latency. For these reasons, Digital Radio over Fibre systems (D-RoF), such as enhanced Common Public Radio Interface (eCPRI) [3] or Open Base Station Architecture Initiative (OBSAI) [4], have been adopted to increase the new wireless network capacity, provide higher data rates at low latency, meet the growing needs for larger transmission bandwidth and guarantees the end-to-end Quality of Service (QoS) [5]. Recently, Radio over Ethernet (RoE) is also broadly investigated [6]. On the other hand, Analog Radio over Fibre (A-RoF) has not yet been standardized. In the literature, C-RAN architecture is proposed for future wireless communications networks to increase the front-haul capacity to reach at least 100 Gbps per cell. The fully centralized architecture is designed to extract the baseband signal, processing functions from Distributed Base Stations (D-BSs) and collocating the BaseBand Units (BBUs) into a pool for centralized signal processing. The C-RAN solution allows for the on-demand deployment, intelligent slicing and can adapt to a wide range of services. It can handle requirements for large bandwidth, short delay and massive connectivity. Moreover, BBU contains resource pooling is implemented to improve resource utilization and to expand network capacity. As depicted in Fig.1, in 5G C-RAN architecture, the BBU functionality is split into two functional units; a Centralized Unit (CU) and a Distributed Unit (DU). The physical location of these units depends on the specific architecture and geographical locations available. In a centralized 5G cloud RAN the DU is hosted in an Edge cloud data center or Central Office (CO) and the CU can be collocated with the DU or hosted in a regional cloud data center. In a distributed 5G cloud RAN architecture the DU is collocated with the radio unit. The Core Network (CN) is connected to the CU via Back-haul network. CU and DU is connected via a Mid-haul network and finally, the Remote Radio Unit (RRU) is connected to DU via Single Mode Fibre (SMF) that has the advantages of low attenuation, high capacity, flexibility and scalability because it allows multi-service operation and independent infrastructure providers. Nevertheless, non-linear optical components and optical Kerr effect, defined as a fibre non-linearity due to changes in the refractive index, including Self-Phase Modulation (SPM) and Cross-

Phase Modulation (XPM) represent the major limitation of increasing the optical system capacity. As a result, nonlinearity compensation is a crucial component of the Radio over Fibre (RoF) system. Therefore, several digital nonlinear equalization algorithms have been proposed for the nonlinear distortion compensation, such as Volterra Nonlinear Equalizer (VNLE) [7], Digital Back Propagation (DBP) [8] and Phase Conjugated Twin-Waves (PCTW) [9]. VNLE has lower complexity and more ability to model complex time-dispersive nonlinear functions [10]. Moreover, several works have addressed the complexity reduction of VNLE for real-time implementations in optical communication systems [11].

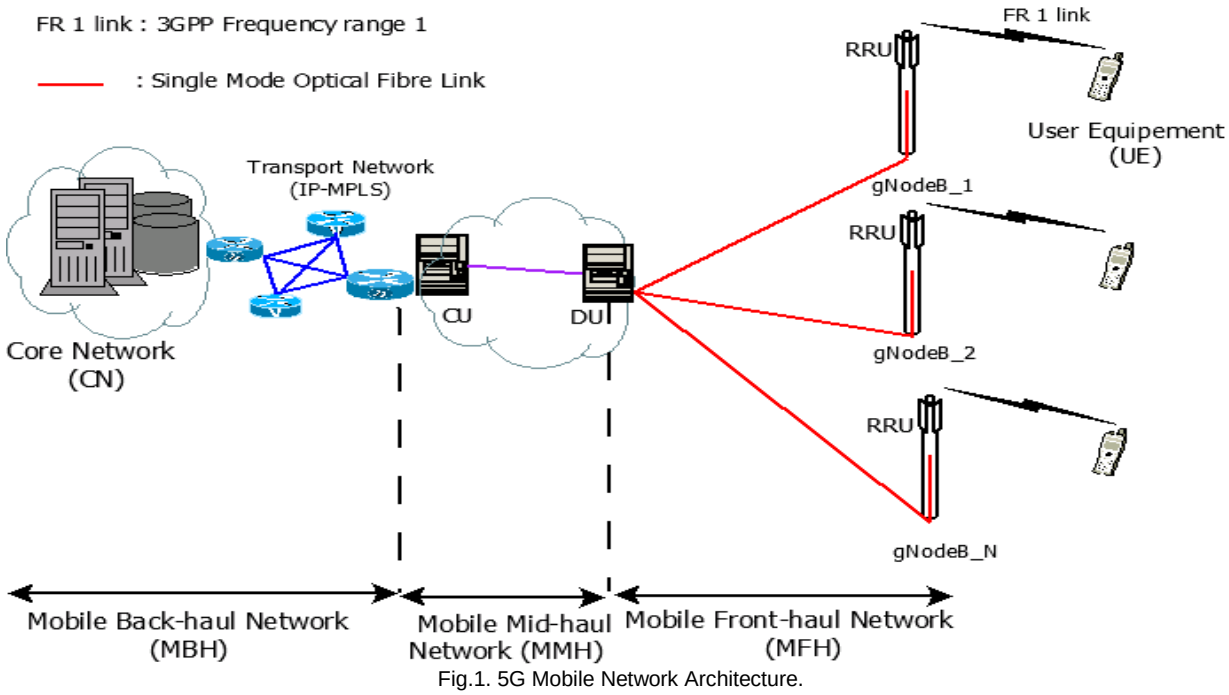

Fig.1. 5G Mobile Network Architecture.

To meet the needs for bandwidth flexibility, higher spectral efficiency and higher bit rate, 5G back-haul and front-haul with more advanced and suitable modulation formats should be developed. Recent research focused on suitable waveforms for the physical layer of 5G wireless network, able to support higher data throughput, greater density for users and provide more efficient utilization of the mm-wave frequency spectrum, and offer several waveforms candidate [12], [13], [14]. Among them; Cyclic Prefix Orthogonal Frequency Division Multiplexing (CP-OFDM), Generalized Frequency Division Multiplexing (GFDM), Filter bank based Multi-Carrier (FBMC) and Universal Filtered Multi-Carrier (UFMC) [15].

In order to increase 5G air interface performance to meet the significantly expanded connectivity needs of the next decade and beyond, there is a need to overcome the limitations that Orthogonal Frequency Division Multiplexing (OFDM) imposes in the traditional multi-carrier system, such as low spectral efficiency, high Out-Of-Band (OOB) emission and strict synchronization requirements. Progress in research activities shows that non-orthogonal digital multicarrier transmission scheme GFDM can provide the required performance for next-generation communication network [16], [17]. GFDM is a flexible digital multicarrier modulation (MCM) technique which gives the possibility to change the characteristics of each subcarrier. It has been defined as a generalization of the traditional OFDM. In fact, GFDM is a block-based modulation scheme that includes a certain number of subcarriers, each one carries a sub-symbol generated in multiple time slots. Moreover, it enables flexible non-rectangular pulse shaping for each subcarrier. Thus, it can control the OOB radiation [18] to provide more robustness for asynchronous transmission by reducing inter-user interference and improve spectral efficiency by reducing the number of required guard carriers. Also, it offers several advantages over OFDM, mainly higher spectral efficiency, lower OOB emission, better performance in Multi-Input Multi-Output (MIMO) multi-path channel [19] and better flexibility of resource allocation due to its fine-granularity sub-block.

Future cellular network requires higher area data throughput to manage the growing demand for wireless data traffic. Indeed, massive MIMO (mMIMO) technology is proposed to achieve this goal by increasing area Spectral Efficiency (SE) (measured in bits/s/Hz/cell) and Energy Efficiency (EE) without an additional base station or extra bandwidth [20]. In a MIMO system, the data rate may be enhanced using various space-time encoding approaches including, Space-Time Block Codes (STBCs), Space-Time Trellis Codes (STTCs), Space-Time Turbo Trellis Codes (STTTC) and Layered Space-Time Codes (LSTC). STBCs have been implemented in MIMO systems to increase the coding gain or diversity gain by coding across multiple antennas over multiple symbol durations, and hence, allowing low complex decoding algorithm based only on linear processing of the received signal. In contrast to STBC, (STTCs) provides both coding gain and diversity gain. It is also more complex than STBC to encode and decode. LSTC schemes provide a trade-off between Spatial Multiplexing (SM) and Spatial Diversity (SD), which is required in certain applications [21]. STBC codes are classified into orthogonal, quasi-

orthogonal and non-orthogonal codes and defined respectively by OSTBC, QOSTBC and non-orthogonal STBC. Each STBC code type has their own benefits and drawbacks that can be determined according to some propriety such as diversity, code gain, rate and complexity of the detector.

Few studies have shown that the GFDM signal is a promising applied technique in the RoF system in the context of the 5th Generation of cellular networks [22], [23]. In [24], the authors succeed in sending four GFDM signals with 10 Gbps, each one 2.5 GHz bandwidth for different carriers 10, 13, 16 and 19 GHz, through 24-km SMF with EVM of 2.6%. Furthermore, the study reported in [25] is focused on GFDM based 5G transceiver at 735 MHz and 26 GHz in Gigabit Passive Optical Networks (GPON) using RoF technology. It demonstrates EVM measurements of 2.18% and 5.7% for 100 Mbps and 1 Gbps, respectively. However, the authors above focused on the RoF link without considering the non-linear effects of the PON components. Experimental results in [16] and [26] report the effectiveness of Time-Reverse Space-Time Code TR-STC GFDM waveform for 2x2 MIMO under Rayleigh channel in terms of flexibility, reduced latency and OOB emission for the smooth migration to the next generation communication network. In [27], the authors proposed a novel receiver with channel equalization and Carrier Frequency Offset (CFO) compensation for STBC MIMO-GFDM under the ITU channel model of 100 km/hr. In [28], an iterative minimum mean squared error with parallel interference cancellation for the MIMO GFDM system has been studied. QOSTBC technique have been heavily studied with OFDM system as well as it never having been implemented to the GFDM system.

To the best of our knowledge, this is the first reported research work of precoded QOSTBC-GFDM and QOSTBC-OFDM signal on fully C-RAN architecture with the integration of the VNLE in the RRU. The main objective of this study is to transmit 16-QAM baseband 4x4 QOSTBC-GFDM (respect. QOSTBC-OFDM) signal already generated in the 5G Central Office (CO) to the RRU then to the User Equipment (UE). In the first phase, the signal is transmitted to the RRU over a 20 km SSMF link. To reduce the Chromatic Dispersion (CD) and the non-linearity effect of the optical fibre link, we propose to use the VNLE based on Recursive Least Squares (RLS) filter in the RRU, then send the signal from the RRU to the UE through a 4x4 MIMO Rayleigh channel [29]. The goal of the system design is to provide a low complexity equalizer algorithm at the UE by the use of the zero-forcing linear equalizer to guarantee low power consumption and to attain low latency communication.

The manuscript is structured in three sections. Section 2 describes the full centralized radio access network architecture from the central office to the user equipment going through the remote radio head. Section 3 provides simulation results of the proposed system using Mean Square Error (MSE), EVM and BER indicators. Finally, conclusion and future work are drawn in section 4.

2. System Description

The developed mathematical model expressions of GFDM waveforms at the transmitter-receiver sides are presented in this section. We also provide a detailed description of space-time coded communication system with N_T=4 transmit antennas and N_R =4 receive antennas, as illustrated in Fig.2.

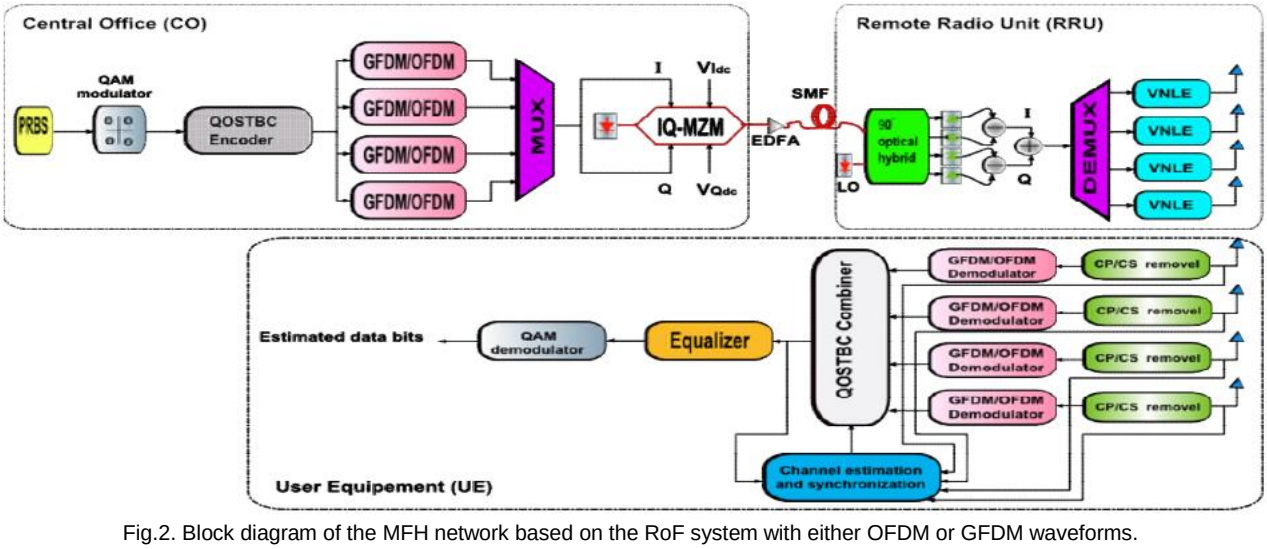

Fig.2. Block diagram of the MFH network based on the RoF system with either OFDM or GFDM waveforms.

2.1. Transmitter

The generated Pseudo-Random Binary Sequence (PRBS) is mapped into a μ-QAM modulation scheme. At each time instant *t*, a block of μ complex data symbol is applied to the QOSTBC encoder. The space-time encoder maps the block of

M symbol input data to $N_T x \mu$ coded data. The quasi-orthogonal codes provide full rate (R=1) and partial orthogonality, which make them attractive because of their achievement of higher code rate than orthogonal codes and lower decoding complexity than non-orthogonal once. The complexity of the QOSTBC does not grow linearly as for STBC but exponentially with the number of transmitting and receiving antennas. In other words, a trade-off between complexity and rate should be considered. According to this, it is efficient to fix $N_T x N_R$ =4x4 because this is the best solution to guarantee a full rate (=1) and reduce the complexity of the receiver, which makes the system more simple and guarantees low latency and low power consumption at the receiver. The QOSTBC is usually presented by a matrix in which each row represents a time slot and each column represents one antenna's transmission over time. Therefore, the encoded data can be expressed as:

$$D = \begin{bmatrix} d_1 & d_2 & d_3 & d_4 \\ -d_2^* & d_1^* & -d_4^* & d_3^* \\ d_3 & d_4 & d_1 & d_2 \\ -d_4^* & d_3^* & -d_2^* & d_1^* \end{bmatrix} \quad (1)$$

We define $C_i, i = 1, 2, 3, 4$ the i[th] column of the matrix D. We can see that

where $< C_i, C_j >= \sum_{l=1}^{N_T} (C_i)_l (C_j)_l^*$ is the inner product of vectors C_i and C_j. Therefore, the subspace created by C_1 and C_4 is orthogonal to the subspace created by C_2 and C_3.

Each column data C_i are modulated by a GFDM block with a length of *N = KM*, including complex data symbols d (k, m), with k = 0… K-1 and *m = 0… M-1*, through K subcarriers and M sub-symbols. To reduce Inter-Symbol Interference (ISI) and OOB leakage, each subcarrier is circularly filtered with a non-rectangular pulse by prototype filter g[n], as illustrated in Fig. 3. The GFDM block is given by [30]

$$X[n] = \sum_{0}^{K-1} \sum_{0}^{M-1} d_{k,m} g_{k,m}, \; n = 0 \ldots N-1 \quad (2)$$

where n denotes the sampling index, and; $g_{k,m}(n) = g\left[(n - mK)_{\bmod N}\right] e^{(-j2\pi \frac{kn}{K})}$ is the mathematical expression of the prototype filter g[n]. There are many types of prototype filters for GFDM waveforms such as Raised Cosine (RC), Root Raised Cosine (RRC), Dirichlet, 1[st] Xia and 4[th] Xia. In this work, the RC has been chosen because it has acceptable interference and also offers the possibility to reduce the OOB radiation. The impulse and frequency response of RC is given by;

$$G_{RC}[f] = \tfrac{1}{2}\left[1 - \cos(lin_\alpha(\tfrac{f}{M}))\right] \quad (3)$$

Where α is the roll-of-factor of the RC filter, M is the number of subsymbols and $lin_\alpha(x)$ is the truncated linear function used to describe the roll-off area defined by α in the frequency domain f and given by the equation below $lin_\alpha(x) = \min(1, \max(0, ((1+\alpha)/2\alpha) + (|x|/\alpha)))$

These filters can be arranged in a transmit matrix A, given by [16]

$$A = (g_{0,0}, g_{1,0} \ldots g_{k-1,0}, g_{0,1} \ldots, g_{K-1,M-1}) \quad (4)$$

In this way, we can write $X = Ad$, where $d = (d_0, \ldots d_{M-1})$.

The GFDM system enables the use of one Cyclic Prefix (CP) and one Cyclic Suffix (CS) per GFDM block, with length N_{cp} and N_{cs}, to avoid Inter-Block-Interference (IBI) caused by the linear and the non-linear effects of the wireless, the photonic devices and the fibre link respectively.

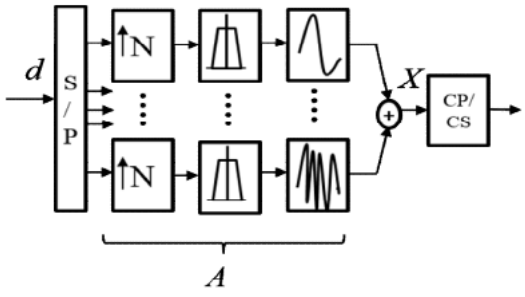

Fig.3. Block diagram of GFDM transmitter.

Some techniques, including Subcarrier Multiplexing (SCM), Mode Division Multiplexing (MDM) and Wavelength Division Multiplexing (WDM), are able to transmit MIMO signals over SSMF. However, these techniques can be considered expensive and complicated to be implemented in practice. Additionally, the number of electrical and optical components increases linearly with the number of MIMO channels in SCM and WDM systems. Moreover, an expensive spatial light modulator is required for the MDM system. For these reasons, Time Division Multiplexing (TDM) can be a potential solution to avoid the above-mentioned problems.

The N_T GFDM signals are combined to one RF signal using TDM and then transmitted to the In-Phase Quadrature Mach Zehnder Modulator (IQ-MZM), shown in Fig.4. The transfer function of the IQ-MZM is given by [11]:

$$E_{out} = E_{in}\left[\gamma\cos\left(\frac{V_I+V_{Idc}}{V_\pi}\pi\right)+j(1-\gamma)\sin\left(\frac{V_Q+V_{Qdc}}{V_\pi}\pi\right)\right] \quad (5)$$

where, $0<\gamma<1$ is the optical splitting ratio with value of 0.55, E_{in} is the optical input field of the Continuous Wave (CW) laser (i.e. $|E_{in}|=1$ in our study), E_{out} is the optical output field, V_{Idc}, V_{Qdc} are the bias voltage of the I and Q arms, respectively. Vπ is the half-wave voltages to provide a πphase shift between the two waveguides, V_I and V_Q are the electric driving voltage of the RF signal. The IQ-MZM is fed by a $\lambda_0 = c/f_0$ = 1550 nm CW Distributed Feedback-Laser (DFB), c is the speed of light in vacuum and f_0 =193.4 THz is the oscillation frequency and biased with the same bias voltage (V_{dc} = V_{Idc}=V_{Qdc}). To achieving intensity modulation, each MZM is operated at the quadrature transmission bias point, with a DC bias of $V_\pi/2$ ($V_\pi = 3V$), which reduces the undesired frequency component generated by the IQ-MZM. The Extinction Ratio (ER) of the optical modulator, which is related to γ, is given by [11]

$$ER(dB) = -20\log_{10}(2\gamma-1) \quad (6)$$

The ER of the modulator is 20 dB, which means that the unwanted sideband can be suppressed approximately by a 20 dB. Finally, the signal is launched at the SSMF.

In the rest of the paper, we will neglect the non-linear effects of the optic devices and will focus only on the non-linear effects caused by the propagation in the optical fibre.

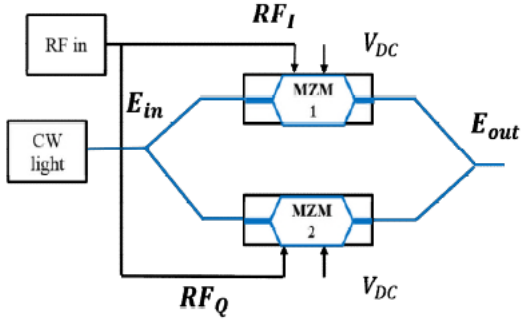

Fig.4. In-Phase Quadrature Mach Zehnder Modulator.

2.2. Optical Fibre Channel Modeling

In this study, Mobile Front-haul (MFH) network based on the SSMF link is considered to carry the information from the CO to the RRU. The Split-Step Fourier Method (SSFM) is a numerical method chosen to model the optical fibre channel in which the link is divided into several sections. Each section is the mathematical solution to the Non-Linear Schrodinger Equation (NLSE), given by [31]

$$E(z+\ell,t) = \exp(\frac{\ell}{2}\hat{D})\exp(\ell\hat{N}\left[E(z+\frac{\ell}{2},t)\right])\exp(\frac{\ell}{2}\hat{D}) \quad (7)$$

where E (z, t) is the complex field envelop of the optical signal at the distance z and time t, ℓ is the step size, $\hat{D} = \frac{i\beta_2\partial^2}{2\partial t^2} - \frac{\theta}{2}$ is the dispersion operator and $\hat{N} = i\sigma|E|^2$ is the nonlinear operator, β_2 describes the first group order velocity dispersion, θ is the fibre attenuation and σ is the nonlinear Kerr coefficient.

In the proposed architecture, the SSMF transmission link has the following parameters; θ =*0.2 dBkm*$^{-1}$,$\beta_2 = -2.10^{-26}S^2M^{-1}$, *PMD= 0.1 ps/km*$^{1/2}$ at the wavelength of 1550 nm with dispersion *17 ps.km.*nm^{-1}, σ=1.2 Wkm^{-1} and the step size, h, is fixed for a length of 1 km for the fibre modeling.

2.3. RRU Conception

At the RRU side, a digital coherent optical receiver is employed to recover the optical signal. The 90° optical hybrid consists of detecting the received optical signal and converting it into the electrical domain. In fact, optical hybrid mixes the received signal with the Local Oscillator (LO) signal in order to achieve the in-phase and the quadrature components of the multiplexed signal. Then, the signal is down-converted to the baseband range. Two possibilities could be adopted; the first one is to apply the VNLE and then de-multiplexing the signal. The second one is to de-multiplex the signal before applying the VNLE for each signal using the parallel processing technique. In this paper, we choose the second solution in order to reduce the complexity of the VNLE and also time latency. Therefore, the signal is passed through a de-multiplexer to recover the MIMO signal. Then, Digital Signal Processing (DSP) block uses VNLE algorithms to compensate for the signal distortion and remove the impairments of the optical channel and photonic devices. In fact, as mentioned in Fig.6, a VNLE based on the RLS algorithm, which has been detailed in [18], is implemented to decrease the influence of Kerr nonlinearity and Chromatic Dispersion (CD) in the optical fibre link. In general, the resulting VNLE output signal y will be very close to the desired GFDM signal mentioned of eq. (2):

$$y = \underbrace{\sum_{i=0}^{N} h_i x(n-i)}_{LE} + \underbrace{\sum_{i=0}^{N}\sum_{j=0}^{N}\sum_{k=0}^{N} h_{i,j,k}(n)x(n-i)x(n-j)x(n-k)}_{NLE} \quad (8)$$

where x is the input signal, hi is the filter coefficients at the i^{th} order kernels of Volterra model and N is the memory length. Equation (8) can be written as: $y = W^H U_n$ (9).
where U_{Nx1} is the input vector which contains N values of x and W_{1xN} is the filter coefficients vector given respectively by the following equations [32].

$$U(n) = \left[x(n)x(n-1),...,x(n-N),...,x^2(n)x^*(n),x^2(n)x^*(n-1),...,x^2(n-N)x^*(n-N)\right]^T \quad (10)$$

$$W^H = \left[h_0(n)h_1(n),...,h_p(n),h_{0,0,0}(n)h_{0,0,1}(n)...,h_{0,N,0}(n)h_{0,N,1}(n)h_{N,N,N}\right] \quad (11)$$

The computational complexity of the VNLE is given by the following formula [11]:

$$CC_{VNLE}(K,N) = \sum_{i=1}^{K}\frac{(N-1+i)!}{(i-1)!(N-1)!} \quad (12)$$

According to equation (9), and as shown in Fig.5 the complexity of the VNLE increased with the order K. Therefore, limiting the number of the VNLE order to K=2 or 3 is a good solution to reduce the number of arithmetical operations and consequently the time latency.

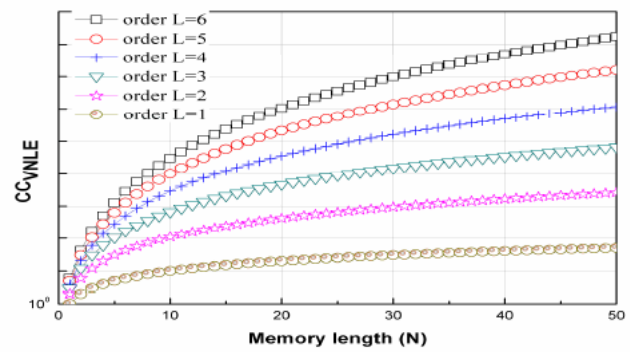

Fig.5. Computational complexity vs. memory length of VNLEs with a different order.

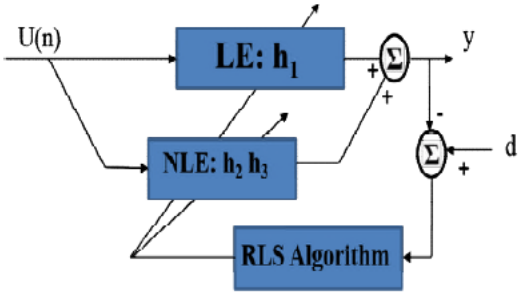

Fig.6. Block diagram of adaptive 3rd order VNLE based on RLS filter.

Among the known techniques to adapt the VNLE, the most recognized are based on RLS and LMS algorithms [33-34]. RLS converges faster than LMS, but it is more computationally intensive in addition to time-varying weakness. In this paper, we limit our analysis to the RLS algorithm because it provides a fast adaptation speed and keeps low latency time in the network. Therefore, the VNLE taps weights can be updated by minimizing the cost function ζ given by

$$\zeta = \sum_{k=0}^{n} \lambda^{n-k} \left[e(k) \right]^2 \quad (13)$$

where λ is the forgetting factor 0<λ≤1, which gives the weight exponentially to error older samples, e (.) is the error function depending on the filter coefficients and defined by :

$$e(k) = d(k) - W^T(k)U(k), k = 0...n; \quad (14)$$

where, d (.) is the desired signal already generated in the transmitter part.

2.4. MIMO Channel Modeling

The output signal from the VNLE is up-converted to the Frequency Range 1 (FR1) defined by the 3rd Generation Partnership Project (3GPP) standard. For the wireless channel design, QOSTB encoding is proposed to improve reliability in data transfer. This technique used in wireless communication to send multiple copies of a data stream across N_T x NR antenna. Therefore, QOSTBC encoder process the incoming complex GFDM symbol and arranges them in a matrix S of the size of N_Tx($N + N_{CP} + N_{CS}$), where each row vector s_i contains data to be transmitted from the transmit antenna N_i and each column includes the symbols to be transmitted on the k^{th} subcarrier and m^{th} sub-symbol. This means that row vectors of S matrix are simultaneously transmitted from the N_T transmit antennas over the MIMO independent flat-fading Rayleigh channel H corrupted by an Additive White Gaussian Noise (AWGN) matrix W. Where H is the channel frequency response containing N_Tx N_R vectors.

2.5. QOSTBC-MIMO GFDM Receiver

At the UE side, the received vector r_k of the k^{th} subcarrier, for an N_T x N_R MIMO Rayleigh channel, can be expressed as [16]:

$$r_k = H_k s_k + w_k, k = 0,1...N-1 \quad (15)$$

where N_T and N_R denote the number of transmitting and receiving antennas respectively, N is number of subcarriers, w_k is the channel noise vector, $H_k$is the N_T x N_R frequency response channel matrix and s_k is transmit data vector at the k^{th} subcarrier.

After CP and CS removal, different linear equalizer (LE) approaches can be used to restore data symbols from the equalized GFDM signal. The GFDM demodulation process can be written as $\hat{d} = Bz$. The LEs that can be used are Zero Forcing (ZF) receiver $B_{ZF} = A^{-1}$, Matched Filter (MF) receiver $B_{MF} = A^H$ and Minimum Mean Square Error (MMSE) receiver $B_{MMSE} = (R_w + A^H A)^{-1} A^H$. According to [35], the complexity of each equalizer is given in the TABLE I. As indicated

in this table, ZF and MF have the same complexity which is less than the complexity of the MMSE. The authors in [36] have shown that ZF is more efficient than MF for the GFDM waveform. Therefore, we use the ZF equalizer in this study in order to build a low complexity GFDM demodulator with acceptable performance. The demodulated signal passed through a QOSTBC combiner with a channel estimation process.

TABLE I
Receiver complexity

Parameters	Complex Multiplication	Complexity
ZF	$N^2 + N\log_2(N) + 2N$	$O(N^2)$
MMSE	$2N^3 + \frac{5}{2}N^2 + \frac{N}{2}$	$O(N^3)$
MF	$N^2 + N\log_2(N) + 2N$	$O(N^2)$

3. Results and Discussion

The generated PRBSs are mapped into a QAM scheme, then converted from Serial to Parallel (S/P) streams. The complex data symbols are encoded with Allamouti 4x4 QOSTBC encoder. At the output, we obtain four quasi-orthogonal signals, each of them modulated with GFDM (respect. OFDM) waveforms. As shown in TABLE II, the total number of subcarrier is 2048 in which 1200 are active subcarriers for each GFDM and OFDM waveforms. In order to avoid ISI and to improve SE, a CP with 12.5% of length, is added for each QOSTBC-GFDM signal (respect. QOSTBC-OFDM). Then, the four QOSTBC-GFDM signals (respect. QOSTBC-OFDM) are multiplexed using the TDM technique. The system operated with a 16-QAM modulation order. In OFDM and GFDM, the SE does not depend on the burst duration and it is a function of the modulation parameters. For GFDM, the SE is higher compared to OFDM as a GFDM symbol is M times longer compared to an OFDM one. Indeed, for GFDM, the SE loss due to the CP insertion is limited as there is one CP per GFDM symbol (i.e. 1 CP per M equivalent OFDM symbols).In this section, we present the simulation results to illustrate and verify the BER and EVM of precoded QOSTBC-GFDM and QOSTBC-OFDM under 4x4 MIMO Rayleigh fading channel.

TABLE .II
Simulation parameters for both GFDM and OFDM block

Parameters	GFDM	OFDM
Number of subcarriers, K	2048	2048
Active subcarriers, Kon	1200	1200
Number of time slots, M	3	1
Active time slots, Mon	3	1
Pulse shape filter, g	RC	Rect
Roll-off factor, α	0.1	0
Length of CP, N_{CP}	768	256
Modulation order, μ	4	4
Sampling frequency, Fs (MHz)	170.67	170.67
Sampling time, Ts (ns)	5.86	5.86
Bandwidth, Bw (MHz)	100	100
Spectral Efficiency, SE (bit/s/Hz)	8.28	6.82

3.1. Power Spectral Density and PAPR Comparison

In this section, we present the Power Spectral Density (PSD) of OFDM, GFDM, QOSTBC-OFDM and QOSTBC-GFDM waveforms. In addition, we compute the Complementary Cumulative Distributed Function (CCDF) of the Peak-to-Average-Power (PAPR) (Fig.8) for the considered waveforms. As shown in fig.7, GFDM has a slightly lower OOB leakage compared to OFDM. Moreover, the OOB emission results conveyed that QOSTBC-GFDM and QOSTBC-OFDM have a low OOB emission compared to GFDM and OFDM respectively. Therefore, applying the QOSTBC encoder results in approximately 7.8 dB reduction in the OOB radiation compared to GFDM and 10.8 dB compared to OFDM. The PAPR is a metric to describe the envelope fluctuation dynamics of the transmitted signal. The CCDF is defined as the probability that PAPR exceeds a certain value of $PAPR_0$. It is interesting to note that PAPR of GFDM is worse than that of OFDM, for example, for a probability (P) of 10^{-3}, the gap between OFDM and GFDM waveform is small, around 0.3 dB. This is because of the high roll of factor values and the self-inflicted interference due to the loss of orthoganlity between subcarriers caused by the pulse shaping operation. Moreover, it should be noted that, applying QOSTBC encoder for OFDM and GFDM waveforms do not change the CCDF of the PAPR curves.

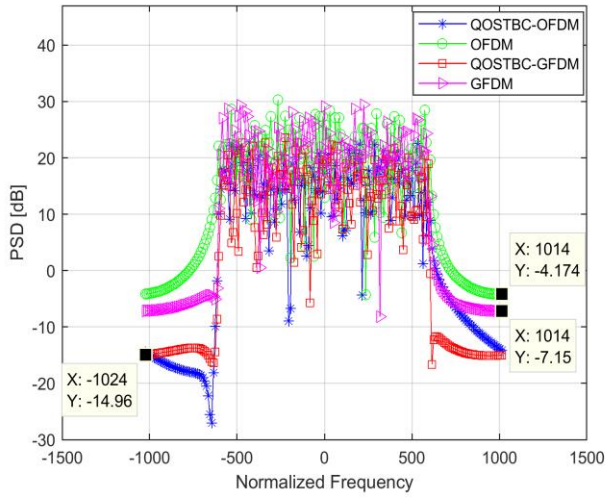

Fig 7. PSD of the waveforms

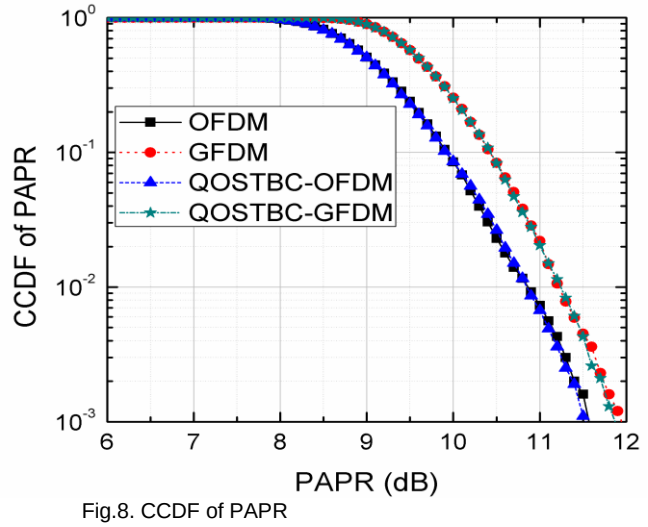

Fig.8. CCDF of PAPR

3.2. Optical Back-to-Back Configuration

To highlight the impact of optical fibre on the transmitted signal, we assume that the CO is directly connected to the RRU, i.e., an optical Back to Back (B2B) connection between the DU and the RRU and thus QOSTBC-GFDM (respect. QOSTBC-OFDM) signals are directly connected to the antenna site. This method allows us to neglect the harmful effects of photonic devices and optical fibre channel, including attenuation, non-linearity, chromatic dispersion and polarization mode dispersion. Fig.9 shows the impact of the MIMO Rayleigh free-space channel on both OFDM and GFDM signals. Fig.9.(a) shows that the BER value is almost zero at an SNR equal to 4 dB, 12 dB and 17 dB for both GFDM and OFDM signals in the case of 4-QAM, 16-QAM and 64-QAM, respectively. Fig.9. (b) illustrates that the EVM for both signals and for each modulation order reaches ~ 4% at 20 dB SNR. These results prove that QOSTBC-OFDM and QOSTBC-GFDM waveforms have approximately the same performance in terms of BER and EVM under a 4x4 MIMO Rayleigh channel. Next sections, we will discuss the effect of the IQ-MZM and optical fibre link to the signal quality.

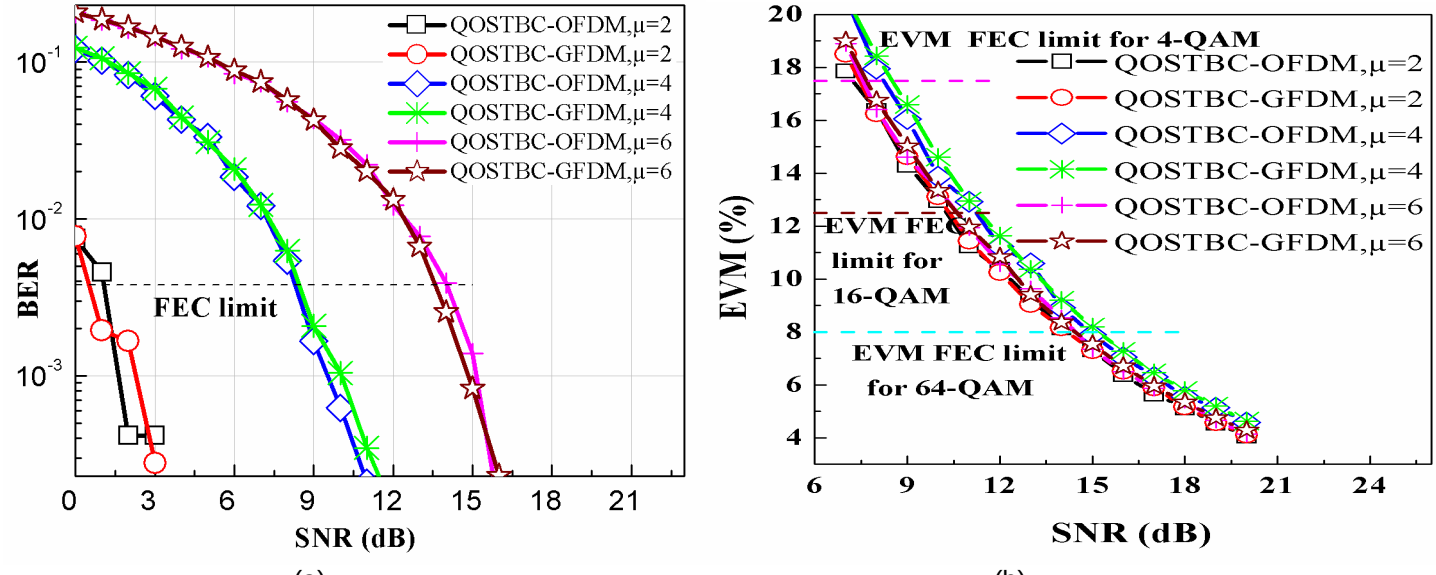

(a) (b)

Fig.9. (a) BER and (b) EVM comparison between QOSTBC-OFDM and QOSTBC-GFDM waveforms on B2B optical fibre configuration.

3.3. Short-Haul Transmission

In Fig.10, the measured PSD of QOSTBC-OFDM and QOSTBC-GFDM signals before and after the IQ-MZM are shown. The non-linearity effect of the IQ-MZM is clear. In fact, IQ-MZM caused harmonics of the signal OOB emission. Thus, for example, in a QOSTBC-GFDM, the OOB noise power of QOSTBC-GFDM and QOSTBC-OFDM before the IQ-MZM, see Fig.10.(a)-(b), is 10 dB and 5 dB lower than the OOB noise of QOSTBC signals after IQ-MZM, respectively. All these results show that IQ-MZM increases the OOB noise level through its non-linearity effect. Indeed, filtering at the receiver side is required to reduce the OOB noise level and compensate non-linearity.

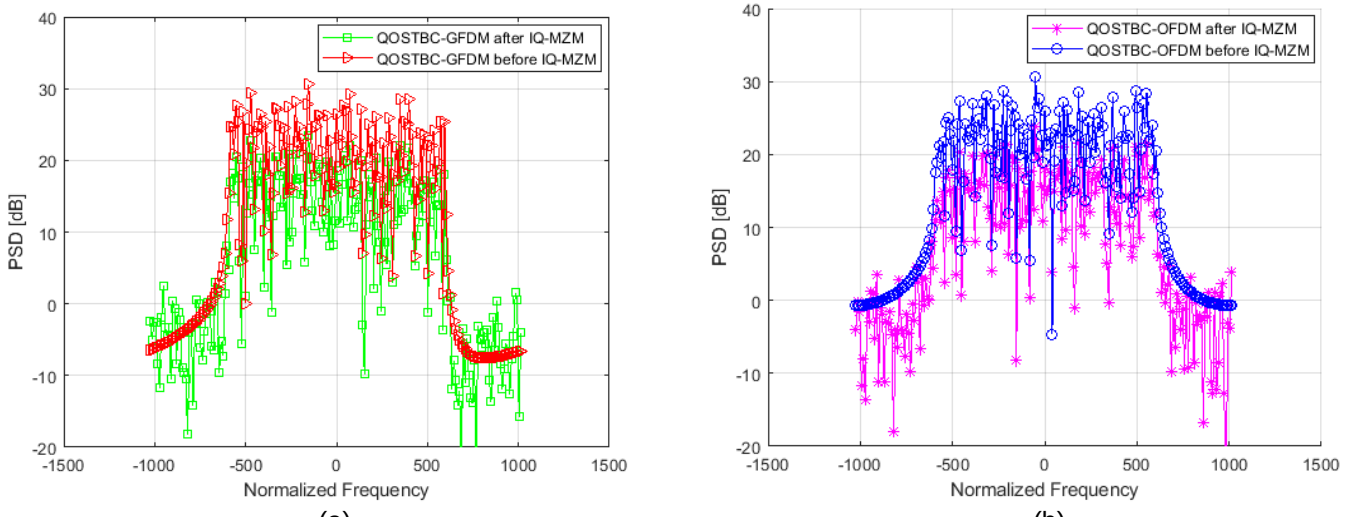

(a) (b)

Fig.10. PSD of (a) QOSTBC OFDM before and after IQ-MZM (b) QOSTBC-GFDM before and after IQ-MZM.

In Fig.11, it is observed that the MSE values obtained for QOSTBC-OFDM signal are lower than those of the QOSTBC-GFDM signal for a Launched Optical Power (LOP) varies between –2 dBm and 16 dBm and for an optical fibre length varies from 10 km to 40 km. Increasing the fibre length reduces the ability of the VNLE to reconstruct the original signal from the received signal. This can be explained by the importance of the ISI phenomenon, which deteriorates the GFDM signal due to the non-orthogonality of the GFDM symbol compared to that of the OFDM. Fig.10 shows that the minimum error of both OFDM and GFDM signal obtained at 8 dBm, and then increased exponentially. Therefore, we define the linear region before the 8 dBm and the non-linear region after this point. For example, at 8 dBm LOP and for 20 km fibre length, MSE reaches -18.24 dB and -18.19 dB for QOSTBC-OFDM and QOSTBC-GFDM, respectively. It is seen that the error increases with increasing the fibre length because the non-linearity effects become clearly higher, especially in the nonlinear region. As expected, the presented results show that the 3rd order VNLE with five taps is more efficient than both VNLE first and third taps. Indeed, increasing the VNLE taps improves the performance of the transmission link by reducing the mean square error between the original signal and the output signal from the VNLE. For example, for a 20 km fibre length at 8 dBm LOP, increasing VNLE from 1 tap to 3 taps and from 3 to 5 taps increases the MSE by 0.47 dB and 0.32 dB, respectively. On the other hand, increasing VNLE taps lead to an exponential increase in the computational complexity of the system. Consequently, the time latency becomes increasingly important. Therefore, high-speed electronic devices should be implemented to ensure the low latency criteria in the system.

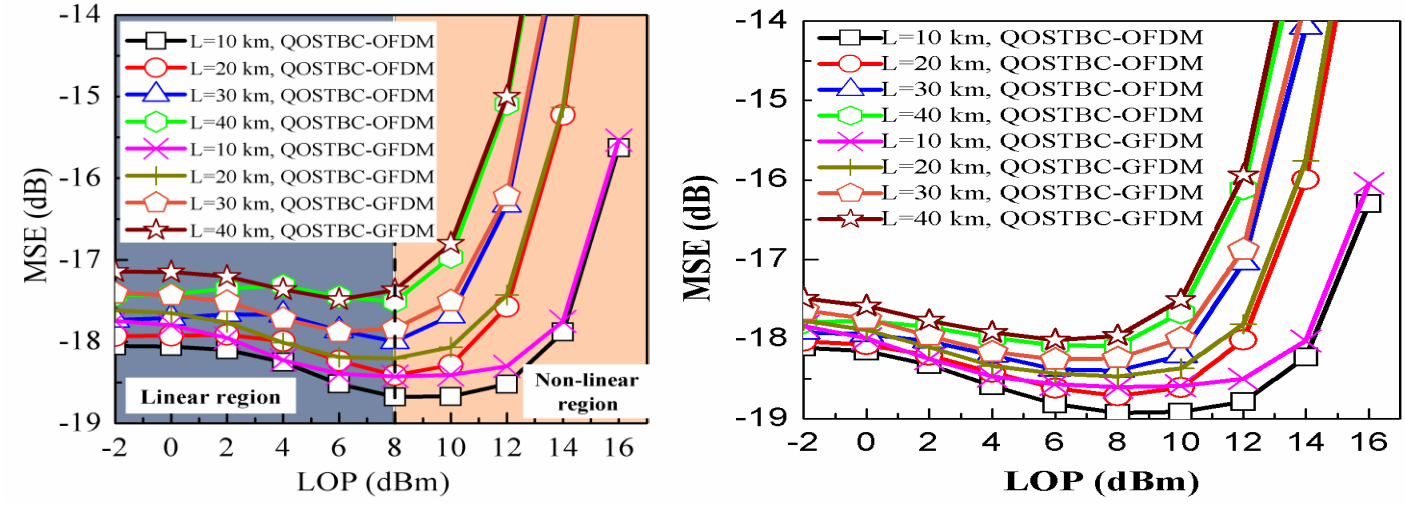

(a) **(b)**

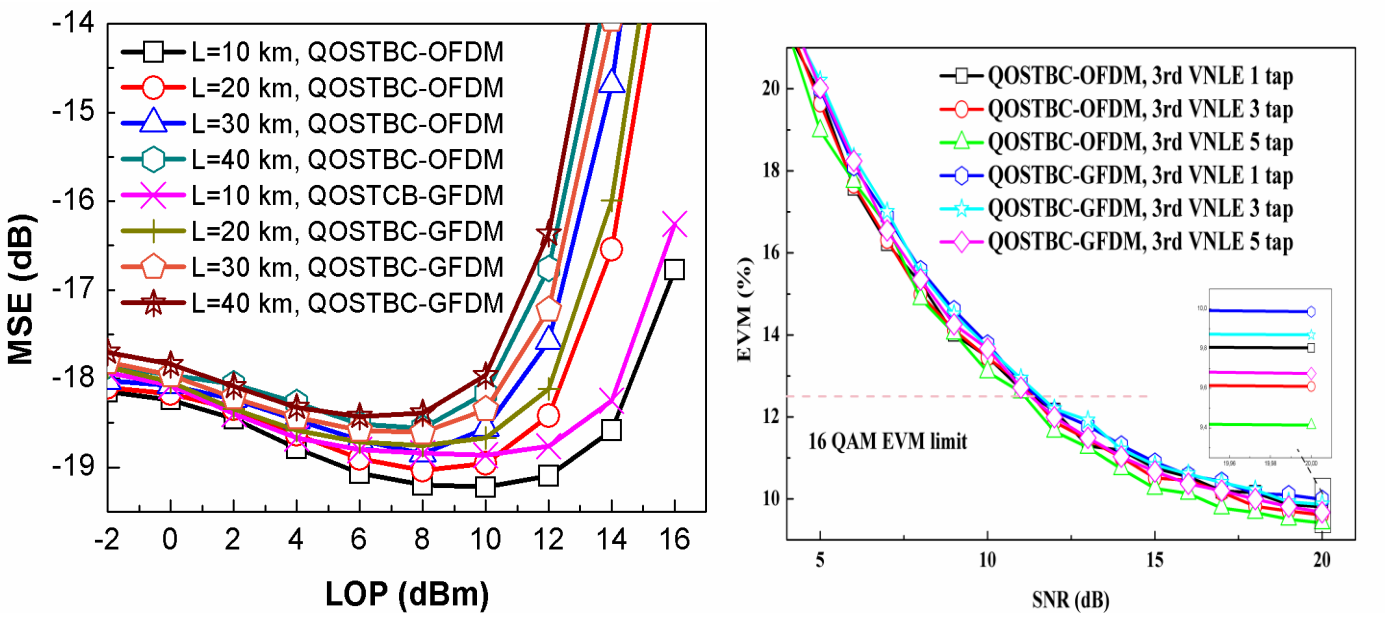

Fig.11. Minimum mean square error vs. launched optical power after third-order VNLE (a) one-tap (b) three taps (c) five taps and (d) error vector magnitude against SNR.

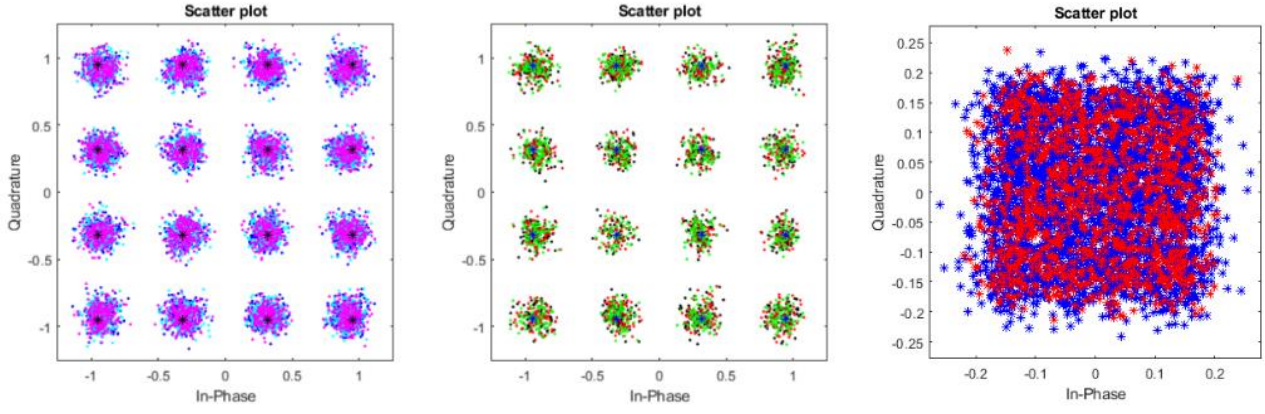

Fig.12. Constellation diagram of 16-QAM (a) GFDM (b) OFDM for one, three and five taps third-order VNLE (c) OFDM (red) and GFDM (blue) without VNLE at RRU.

The results of fig 11.(d), 1.2(a) and 12.(b) show that the EVM performance of both QOSTBC-OFDM and QOSTBC-GFDM has been significantly improved compared to the result of Fig 12. (c) without using VNLE equalizer. However, the same obtained results degraded in comparison with the results already mentioned in section 3.1 (Optical B2B configuration). The propagation of signals in the optical channel affects and decreases the EVM performance by ~ 6% at 20 dB SNR (from 4% in B2B propagation to 10% in the short-haul link). Therefore, Polarization Mode Dispersion (PMD) and non-linear impairments of IQ-MZM and optical fibre devices are the major parameters that effect signal quality. It is shown that the VNLE equalizers with different taps have almost the same performance for both QOSTBC-OFDM and QOSTBC-GFDM waveforms with preference to 3 taps VNLE. These results confirm that VNLE affect signal quality significantly.

4. Conclusion

We have developed and demonstrated, using numerical simulation, a front-haul RoF system based on novel waveforms for next-generation network communication with low complexity equipment receivers. The proposed architecture applies coherent RoF technology to transmit 16-QAM QOSTBC-GFDM and QOSTBC-OFDM signals from the central office to the remote radio head through a single-mode fibre. Furthermore, third-order VNLE based on RLS filter has been implemented for the first time in the RRU, to compensate for fibre non-linearity effects. We evaluated and compared the BER and EVM performance of the system with QOSTBC-OFDM and QOSTBC-GFDM, in the short-haul optical fibre transmission link. Simulation results show that the proposed QOSTBC-GFDM suffers from a small degradation in EVM performance as QOSTBC-OFDM due to the non-orthogonal subcarriers. Our study also shows that the proposed RoF system architecture represents a promising solution to improve the performance of 5G and beyond wireless communication system performance

with low complexity receivers significantly. Additionally, our proposed fully centralized RoF system has significant advantageous on receiver power consumption optimization and effective improvement on network latency.

References

[1] C.-X. Wang et al., "Cellular architecture and key technologies for 5G wireless communication networks," IEEE Commun. Mag., vol. 52, no. 2, pp. 122–130, Feb. 2014.

[2]https://futurenetworks.ieee.org/images/files/pdf/ieee-5g-roadmap-white-paper.pdf.

[3]J. Bartelt et al., "5G transport network requirements for the next generation fronthaul interface," J Wireless Com Network, vol. 2017, no. 1, p. 89, Dec. 2017.

[4]A. Pizzinat, P. Chanclou, F. Saliou, and T. Diallo, "Things You Should Know About Fronthaul," J. Lightwave Technol., vol. 33, no. 5, pp. 1077–1083, Mar. 2015.

[5]L. Chen, X. Lei, S. Wen, and J. Yu, "A novel radio over Fibre system with DWDM mm-wave generation and wavelength reuse for upstream data connection," *Opt. Express, OE*, vol. 15, no. 9, pp. 5893–5897, Apr. 2007.

[6] G. Otero Pérez, D. Larrabeiti López, and J. A. Hernández, "5G New Radio Fronthaul Network Design for eCPRI-IEEE 802.1CM and Extreme Latency Percentiles," IEEE Access, vol. 7, pp. 82218–82230, 2019.

[7] L. Chen, J. Xiao, and J. Yu, "Application of Volterra Nonlinear Compensation in 75-GHz mm-Wave Fiber-Wireless System," IEEE Photonics Journal, vol. 9, no. 1, pp. 1–7, Feb. 2017.

[8] Q. Zheng, L. Huang, W. Li, Q. Feng, C. Fu, and J. Yu, "NSNI Mitigation in Bi-Directional Raman Amplified Unrepeatered System Using Split-DBP," Journal of Lightwave Technology, vol. 36, no. 16, pp. 3494–3501, Aug. 2018.

[9] J. S. Tavares, L. M. Pessoa, and H. M. Salgado, "Nonlinear Compensation Assessment in Few-Mode Fibers via Phase-Conjugated Twin Waves," *Journal of Lightwave Technology*, vol. 35, no. 18, pp. 4072–4078, Sep. 2017.

[10]E. Giacoumidis, J. Wei, I. Aldaya, C. Sanchez, H. Mrabet, and L. P. Barry, "Fiber-induced nonlinearity compensation in coherent optical systems by affinity propagation soft-clustering," arXiv:1812.05600 [eess], Dec. 2018.

[11] N.-P. Diamantopoulos, H. Nishi, W. Kobayashi, K. Takeda, T. Kakitsuka, and S. Matsuo, "On the Complexity Reduction of the Second-Order Volterra Nonlinear Equalizer for IM/DD Systems," Journal of Lightwave Technology, vol. 37, no. 4, pp. 1214–1224, Feb. 2019.

[12] A. Hammoodi, L. Audah, and M. A. Taher, "Green Coexistence for 5G Waveform Candidates: A Review," *IEEE Access*, vol. 7, pp. 10103–10126, 2019.

[13]Y. Liu *et al.*, "Waveform Design for 5G Networks: Analysis and Comparison," *IEEE Access*, vol. 5, pp. 19282–19292, 2017.

[14] I. B. F. de Almeida, L. L. Mendes, J. J. P. C. Rodrigues, and M. A. A. da Cruz, "5G Waveforms for IoT Applications," *IEEE Communications Surveys Tutorials*, vol. 21, no. 3, pp. 2554–2567, thirdquarter 2019, doi: 10.1109/COMST.2019.2910817.

[15]R. Gerzaguet et al., "The 5G candidate waveform race: a comparison of complexity and performance," EURASIP Journal on Wireless Communications and Networking, vol. 2017, p. 13, Jan. 2017.

[16]N. Michailow et al., "Generalized Frequency Division Multiplexing for 5th Generation Cellular Networks," IEEE Transactions on Communications, vol. 62, no. 9, pp. 3045–3061, Sep. 2014.

[17]Y. Li, K. Niu, and C. Dong, "Polar-Coded GFDM Systems," *IEEE Access*, vol. 7, pp. 149299–149307, 2019.

[18]D. Zhang, M. Matthé, L. L. Mendes, and G. Fettweis, "A Study on the Link Level Performance of Advanced Multicarrier Waveforms Under MIMO Wireless Communication Channels," IEEE Transactions on Wireless Communications, vol. 16, no. 4, pp. 2350–2365, Apr. 2017.

[19]J. Zhong, G. Chen, J. Mao, S. Dang, and P. Xiao, "Iterative Frequency Domain Equalization for MIMO-GFDM Systems," IEEE Access, vol. 6, pp. 19386–19395, 2018.

[20]Z. Chen, F. Sohrabi, and W. Yu, "Multi-Cell Sparse Activity Detection for Massive Random Access: Massive MIMO Versus Cooperative MIMO," IEEE Transactions on Wireless Communications, vol. 18, no. 8, pp. 4060–4074, Aug. 2019.

[21]Jian Cheng, Haifeng Wang, Ming Chen, and Shixin Cheng, "Performance comparison and analysis between STTC and STBC," in IEEE 54th Vehicular Technology Conference. VTC Fall 2001. Proceedings (Cat. No.01CH37211), Atlantic City, NJ, USA, 2001, vol. 4, pp. 2487–2491.

[22]F. Tian et al., "A Novel Concatenated Coded Modulation Based on GFDM for Access Optical Networks," IEEE Photonics Journal, vol. 10, no. 2, pp. 1–8, Apr. 2018.

[23] M. Rico-Martinez, C. C. C. Vasquez, S. I. Rodriguez, G. M. V. Duran, and I. T. Monroy, "Comparison of performance between OFDM and GFDM in a 3.5GHz band 5G hybrid Fiber-Wireless link using SDR," in *2018 International Topical Meeting on Microwave Photonics (MWP)*, 2018, pp. 1–4, doi: 10.1109/MWP.2018.8552915.

[24]M. Chen et al., "Multi-broadband radio over fiber system based on Generalized Frequency Division Multiplexing," in 2016 15th International Conference on Optical Communications and Networks (ICOCN), 2016, pp. 1–3.

[25] R. M. Borges *et al.*, "Integration of a GFDM-Based 5G Transceiver in a GPON Using Radio Over Fiber Technology," *Journal of Lightwave Technology*, vol. 36, no. 19, pp. 4468–4477, Oct. 2018, doi: 10.1109/JLT.2018.2826483.

[26]M. Danneberg et al., "Implementation of a 2 by 2 MIMO-GFDM transceiver for robust 5G networks," in 2015 International Symposium on Wireless Communication Systems (ISWCS), 2015, pp. 236–240.

[27]Y.-K. Chang, F.-B. Ueng, and K.-Z. Wu, "A novel MIMO-GFDM receiver for next generation communication," Transactions on Emerging Telecommunications Technologies, vol. 29, no. 6, p. e3288, 2018.

[28]M. Matthé, D. Zhang, and G. Fettweis, "Low-Complexity Iterative MMSE-PIC Detection for MIMO-GFDM," IEEE Transactions on Communications, vol. 66, no. 4, pp. 1467–1480, Apr. 2018.

[29]D. Tse and P. Viswanath, Fundamentals of Wireless Communication. Cambridge: Cambridge University Press, 2005.

[30] A. Farhang, N. Marchetti, and L. E. Doyle, "Low-Complexity Modem Design for GFDM," *IEEE Transactions on Signal Processing*, vol. 64, no. 6, pp. 1507–1518, Mar. 2016.

[31] O. V. Sinkin, R. Holzlohner, J. Zweck, and C. R. Menyuk, "Optimization of the split-step Fourier method in modeling optical-Fibre communications systems," *Journal of Lightwave Technology*, vol. 21, no. 1, pp. 61–68, Jan. 2003.

[32]N. Mallouki et al., "Analysis of full Volterra nonlinear equalizer for downlink LTE system", in 2015 Wireless Telecommunications Symposium (WTS), 2015, pp. 1–6.

[33]V. H. Nascimento and Y. V. Zakharov, "RLS Adaptive Filter With Inequality Constraints," IEEE Signal Processing Letters, vol. 23, no. 5, pp. 752–756, May 2016.

[34] Mohd. T. Khan and R. A. Shaik, "Optimal Complexity Architectures for Pipelined Distributed Arithmetic-Based LMS Adaptive Filter," IEEE Transactions on Circuits and Systems I: Regular Papers, vol. 66, no. 2, pp. 630–642, Feb. 2019.

[35]W. D. Dias, L. L. Mendes, and J. J. P. C. Rodrigues, "Low complexity GFDM receiver for Frequency-Selective Channels," IEEE Communications Letters, pp. 1–1, 2019.

[36]A. Farhang, N. Marchetti, and L. E. Doyle, "Low complexity GFDM receiver design: A new approach," in 2015 IEEE International Conference on Communications (ICC), 2015, pp. 4775–4780.